Available online at www.sciencedirect.com

SciVerse ScienceDirect

Ceramics International 39 (2013) 2117–2121

CERAMICS INTERNATIONAL

www.elsevier.com/locate/ceramint

Short communication

Low-temperature sintering effect on varistor properties of $ZnO–V_2O_5–MnO_2–Nb_2O_5–Bi_2O_3$ ceramics

Choon-W. Nahm*

Semiconductor Ceramics Laboratory, Department of Electrical Engineering, Dongeui University, Busan 614-714, Republic of Korea

Received 17 June 2012; accepted 5 July 2012
Available online 14 July 2012

Abstract

The microstructure and electrical properties of the $ZnO–V_2O_5–MnO_2–Nb_2O_5–Bi_2O_3$ varistor ceramics were systematically investigated at different sintering temperatures (875–950 °C). The average grain size increased remarkably in the range of 5.4 to 15.0 μm with an increase in the sintering temperature. The sintered density of pellets decreased from 5.50 to 5.34 g/cm^3 as the sintering temperature increased. The breakdown field decreased noticeably from 5785 to 1181 V/cm with an increase in the sintering temperature. The varistor ceramics sintered at 900 °C exhibited excellent nonlinear properties, in which the nonlinear coefficient is 61.5 and the leakage current density is 14.1 μA/cm^2.

Keywords: A. Sintering; C. Electrical properties; D. ZnO; E. Varistors

1. Introduction

As semiconductor devices are gradually miniaturized and electronic circuit densities are gradually increased, the electronic systems will have a greater susceptibility to transients such as lightning, nuclear electromagnetic pulse, high energy switching, or electrostatic discharge. A varistor is a semiconductor device protecting electronic circuits from transient overvoltage.

ZnO varistors are semiconducting electroceramic devices formed by sintering ZnO powder doped with minor additives, which are composed of inherent varistor-former and characteristics-enhancer [1]. They exhibit symmetric *V–I* curves similar to a back-to-back Zener diode [2,3]. ZnO varistors are extensively used in the field of overvoltage protection systems from an electronic apparatus to electrical power systems [2,3].

Commercial multilayered chip varistor ceramics have no choice but to be co-fired with an expensive refractory Pd or Pt as an inner-electrode because they reveal a desirable sinterability at a relatively temperature above 1000 °C, What kinds of ceramics can use cheap Ag instead of Pd or Pt? One candidate is V_2O_5-doped ZnO ceramics by liquid phase sintering, based on melting point (960 °C) of Ag [4,5]. At present, $ZnO–V_2O_5$-based ceramics are being studied for altogether multiplayer chip varistors, unlike Bi_2O_3- and Pr_6O_{11}-doped ZnO ceramics varistor ceramics. A study of V_2O_5-doped ZnO ceramics is yet in its early stages in many points [6–14]. Furthermore, they possess many problems for solution: complex microstructure, low nonlinear coefficient, high leakage current, high dielectric dissipation factor, low stability, etc. [8–14]. The specific additives and the sintering process enable V_2O_5-doped ZnO ceramics to exhibit stronger nonlinear properties. Therefore, it is very important to investigate the effects of sintering process on electrical properties for the varistor ceramics with specified composition. In this study, the low-temperature sintering effect on microstructure and electrical properties of the $ZnO–V_2O_5–MnO_2–Nb_2O_5–Bi_2O_3$ varistor ceramics was investigated, and surprisingly high nonlinear coefficient and noticeably lower leakage current was attained by a proper sintering temperature.

2. Experimental procedure

Highly purity (>99.9%) reagent-grade raw materials with the proportion of 97.375 mol% ZnO+0.5 mol% V_2O_5+2.0

*Tel.: +82 51 890 1669; fax: +82 51 890 1664.
E-mail address: cwnahm@deu.ac.kr

0272-8842/$36.00
http://dx.doi.org/10.1016/j.ceramint.2012.07.025

mol% MnO_2+0.1 mol% Nb_2O_5+0.025 mol% Bi_2O_3 were prepared. Raw materials were mixed by ball milling with zirconia balls and acetone in a polypropylene bottle for 24 h. The mixed slurry was dried at 120 °C for 12 h. The dried mixture was mixed by a magnetic stir bar into a beaker with acetone and 0.8 wt% polyvinyl butyral binder of powder weight. After drying, the mixture was granulated by sieving through a 100-mesh screen to produce starting powder. The sieved powder was pressed into a disk-shaped pellet of 10 mm diameter and 1.5 mm thickness at a pressure of 100 MPa. The pellets were set on MgO plate into alumina sagger and sintered at four temperatures (875 °C, 900 °C, 925 °C, and 950 °C) in air for 3 h, and furnace-cooled to room temperature. The heating and cooling rates were 4 °C/min. The final pellets were about 8 mm in diameter and 1.0 mm in thickness. Conductive silver paste was coated by screen-printing techniques on both faces of the pellets and the electrodes were formed by heating it at 550 °C for 10 min. The electrodes were 5 mm in diameter. Finally, after the lead wire is soldered to both electrodes, the samples were packaged by dipping it into a thermoplastic resin powder.

Both surfaces of the sintered pellets were lapped and ground with SiC paper and polished with 0.3 μm-Al_2O_3 powders to a mirror-like surface. The polished pellets were chemically etched into 1 $HClO_4$:1000 H_2O for 25 s at 25 °C. The surface microstructure was examined using a field emission scanning electron microscope (FESEM, Quanta 200, FEI, Brno, Czech). The average grain size (d) was determined by the linear intercept method [15]. The crystalline phases were identified using an X-ray diffractometer (XRD, X′pert-PRO MPD, Panalytical, Almelo, the Netherlands) with Ni-filtered CuK_α radiation. The sintered density (ρ) was measured using a density determination kit (238490) attached to a balance (AG 245, Mettler Toledo International Inc., Greifensee, Switzerland).

The electric field–current density (E–J) characteristics were measured using a V–I source (Keithley 237, Keithley Instruments Inc., Cleveland, OH, USA). The breakdown field (E_B) was measured at a current density of 1.0 mA/cm^2 and the leakage current density (J_L) was measured at $0.80E_B$. The nonlinear coefficient (α) was calculated from $\alpha=(\log J_2–\log J_1)/(\log E_2–\log E_1)$, where E_1 and E_2 are the electric fields corresponding to $J_1=1.0$ mA/cm^2 and $J_2=10$ mA/cm^2, respectively.

3. Results and discussion

Fig. 1 shows the SEM micrographs of the samples for different sintering temperatures. It can be intuitively seen that the sintering temperature has a noticeable effect on microstructure in terms of the grain size primarily. The uniformity of grain size was significantly improved with an increase in the sintering temperature. The average grain size increased remarkably in the range 5.4–15.0 μm despite small sintering changes with an increase in the sintering temperature. On the whole, the samples show an abrupt increase in the average grain size from 925 °C (see Fig. 4(a) in advance). The density of sintered pellets decreased from 5.5 to 5.34 g/cm^3 corresponding to 95.1–92.4% of the theoretical density (TD) (pure ZnO, TD=5.78 g/cm^3) with

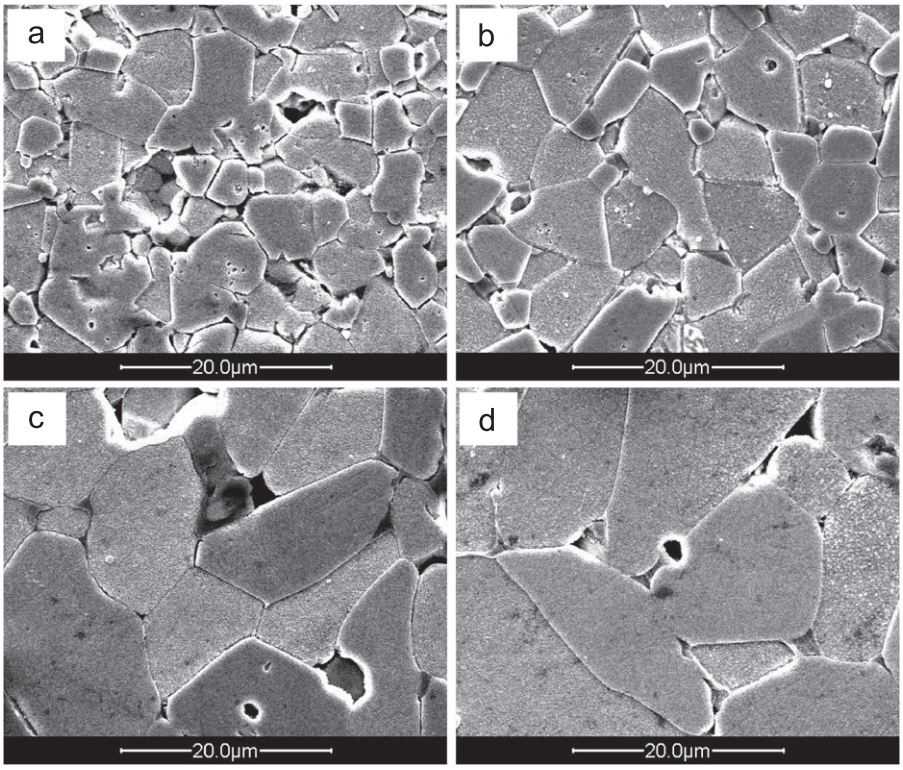

Fig. 1. SEM micrographs of the samples for different sintering temperatures: (a) 875 °C, (b) 900 °C, (c) 925 °C and (d) 950 °C.

Table 1
Microstructure and *E*–*J* characteristic parameters of the samples for different sintering temperatures.

Sintering temperature (°C) for ceramics[b]	d (μm)	ρ[a] (g/cm^3)	E_B (V/cm)	v_{gb} (V/gb)	α	J_L (μA/cm^2)
875	5.4	5.50	5785	3.1	50.3	9.2
900	6.0	5.43	4675	2.8	61.5	14.1
925	11.1	5.37	2233	2.5	34.3	41.8
950	15.0	5.34	1181	1.8	30.1	42.9

[a]Theoretical density 5.78 g/cm^3 for ZnO.
[b]$ZnO+0.5V_2O_5+2.0MnO_2+0.1Nb_2O_5+0.025Bi_2O_3$ (all in mol%).

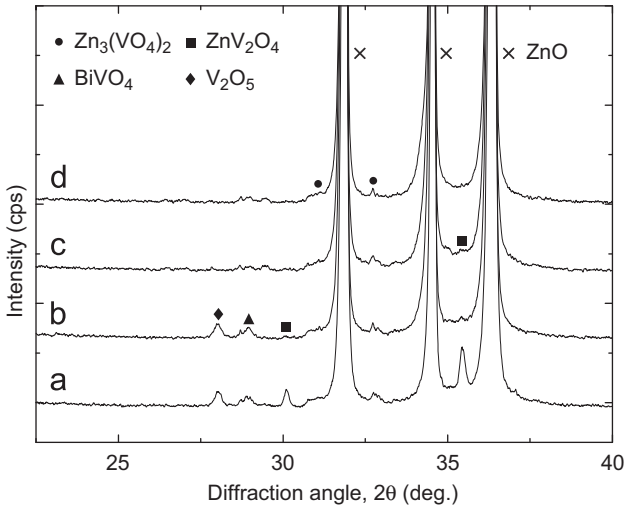

Fig. 2. XRD patterns of the samples for different sintering temperatures: (a) 875 °C, (b) 900 °C, (c) 925 °C and (d) 950 °C.

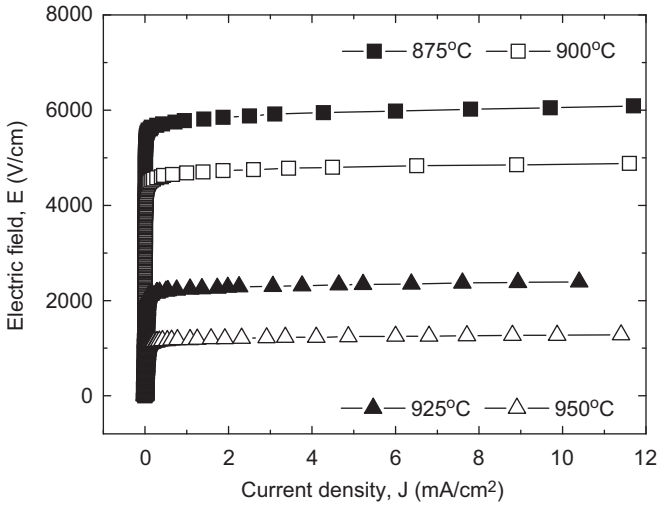

Fig. 3. *E*–*J* characteristics of the samples for different sintering temperatures.

an increase in the sintering temperature. This is attributed to the volatility of the V-species for V_2O_5 with melting point as low as 690 °C (see Fig. 4(b) in advance). The microstructure parameters are summarized in Table 1.

The XRD patterns of the samples for different sintering temperatures are shown in Fig. 2. These patterns revealed the presence of $Zn_3(VO_4)_2$, ZnV_2O_4, $BiVO_4$, and V_2O_5 as minor secondary phases, which act as liquid-phase sintering aids, in addition to a major phase of hexagonal ZnO. The peaks of all minor phases gradually reduced with an increase in the sintering temperature. The minor phases almost disappeared at a sintering temperature beyond 925 °C except for $Zn_3(VO_4)_2$. This is related to the volatility of the V-species, as mentioned previously.

Fig. 3 shows the electric field–current density (*E*–*J*) characteristics of the samples for different sintering temperatures. The varistor properties are featured by the nonlinearity in the *E*–*J* relation. The characteristic curves are composed of two states: one is current-off state before breakdown field and another is current-on state after breakdown field. The *E*–*J* characteristic parameters obtained from *E*–*J* curves are summarized in Table 1.

The behavior of breakdown field (E_B) as a function of sintering temperature was indicated graphically in Fig. 4(c). E_B decreased noticeably from 5785 to 1181 V/cm despite small sintering changes with an increase in the sintering temperature. E_B is predominantly controlled by the grain size (*d*), and slightly depends on the breakdown voltage per grain boundaries (v_{gb}). The breakdown voltage (V_B) is indicated as following expression, $V_B=(D/d)\cdot v_{gb}=n\cdot v_{gb}$ and the E_B is written as following expression, $E_B=v_{gb}/d$, where *d* is the average grain size, *D* is the thickness of sample, and *n* is the number of grain boundaries. Therefore, V_B is proportional to *n* and v_{gb}. In general, to control the breakdown voltage, one has to control the sample thickness for a fixed grain size or alternately one has to control the grain size for constant sample thickness. As a result, the decrease of E_B with an increase in the sintering temperature is attributed to the increase of the average ZnO grain size and the decrease of breakdown voltage per grain boundaries.

The behavior of nonlinear coefficient (α) as a function of sintering temperature was indicated graphically in Fig. 4(d). The α value increased from 50.3 to 61.5 with an increase in the sintering temperature up to 900 °C. However, further increase in the sintering temperature caused nonlinear coefficient to decrease to 30.1 at 950 °C. As a result, it can be seen that the sintering temperature has a

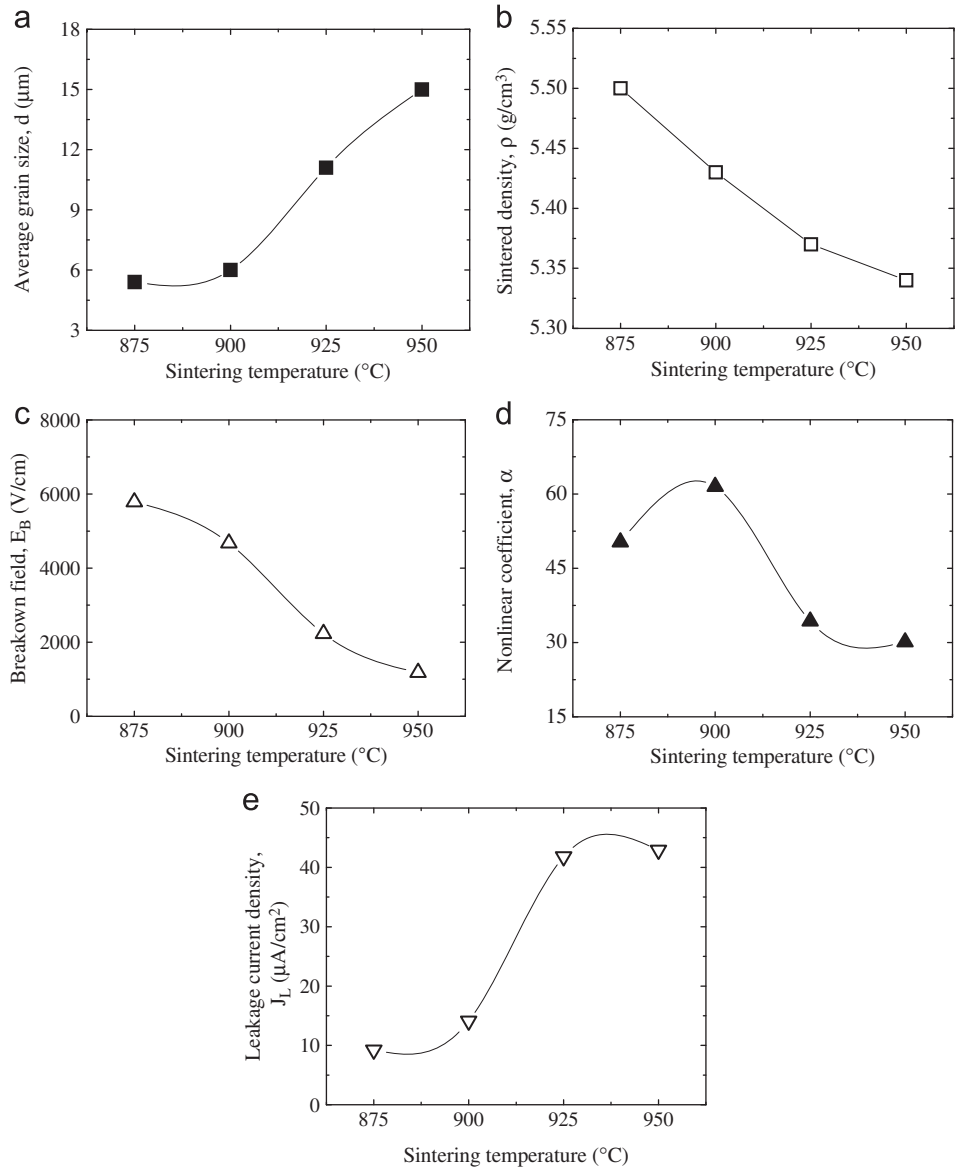

Fig. 4. Microstructure and electrical parameters as a function of sintering temperature: (a) average grain size, (b) sintered density, (c) breakdown field, (d) nonlinear coefficient, and (e) leakage current density.

strong effect on nonlinear properties despite small sintering changes. It should be noted that the sample sintered at 900 °C exhibited an unusual high value ($\alpha = 61.5$) comparable with that of the Er_2O_3-doped ZnO–V_2O_5-based varistors reported until now [14]. In addition, it is remarkable that the sample sintered at a temperature as low as 875 °C exhibited a high value ($\alpha = 50.3$). Therefore, this composition will provide important information in the development of the ZnO–V_2O_5-based varistor ceramics with a high nonlinear coefficient. The behavior of α is strongly related to the potential barrier, which depends on the electronic states related to the zinc vacancies, interstitial zinc, ionized donor-like, oxygen, etc. at the grain boundaries in accordance with the sintering temperature. This is because the sintering temperature varies the density of interface states with the transport of the defect ions toward the grain boundaries. Therefore, the increase or decrease of α with an increase in the sintering temperature is attributed to the increase or decrease of potential barrier height at the grain boundaries.

The behavior of leakage current density (J_L) as a function of sintering temperature was indicated graphically in Fig. 4(e). The J_L value increased from 9.2 to 42.9 μA/cm^2 with an increase in the sintering temperature. On the whole, this system exhibited a much lower leakage current, compared with other ZnO–V_2O_5-based varistor ceramics [11–14]. In particular, the samples sintered at 900 °C exhibited a much lower leakage current density (14.1 μA/cm^2) than that of the ZnO–V_2O_5-based varistors reported until now [11–14]. Note that one of the problems possessed by the ZnO–V_2O_5-based varistor ceramics is a high leakage current. For this reason,

this is a very important result, except that this system exhibits a high nonlinearity ($\alpha = 61.5$), as mentioned earlier.

4. Conclusions

Low-temperature sintering effect on microstructure and electrical properties of the $ZnO–V_2O_5–MnO_2–Nb_2O_5–Bi_2O_3$ varistor ceramics was investigated. The sintered density of pellets decreased due to the volatility of *V*-species with an increase in the sintering temperature. Experimental results indicated that small change in the sintering temperature has a noticeable effect on nonlinear properties. As the sintering temperature increased, the breakdown field decreased due to the increase of grain size. Optimum sintering temperature of this system was found to be 900 °C in terms of nonlinear properties, with the nonlinear coefficient as high as 61.5 and the leakage current density as low as 14.1 $\mu A/cm^2$. It is believed that ZnO–0.5 V_2O_5–2.0 MnO_2–0.1 Nb_2O_5–0.025 Bi_2O_3 (all in mol%) varistor ceramics can be applied to multilayer chip varistor ceramics in the near future.

References

[1] M. Matsuoka, NonOhmic properties of zinc oxide ceramics, Japanese Journal of Applied Physics 10 (1971) 736–746.
[2] L.M. Levinson, H.R. Philipp, Zinc oxide varistor—a review, American Ceramic Society Bulletin 65 (1986) 639–646.
[3] T.K. Gupta, Application of zinc oxide varistor, Journal of the American Ceramic Society 73 (1990) 1817–1840.
[4] J.-K. Tsai, T.-B. Wu, Non-Ohmic characteristics of $ZnO–V_2O_5$ ceramics, Journal of Applied Physics 76 (1994) 4817–4822.
[5] J.-K. Tsai, T.-B. Wu, Microstructure and nonOhmic properties of binary $ZnO–V_2O_5$ ceramics sintered at 900 °C, Materials Letters 26 (1996) 199–203.
[6] H.-H. Hng, K.M. Knowles, Micro-structure and current–voltage characteristics of multicomponent vanadium-doped zinc oxide varistors, Journal of the American Ceramic Society 83 (2000) 2455–2462.
[7] H.-H. Hng, P.L Chan, Effects of MnO_2 doping in V_2O_5-doped ZnO varistor system, Materials Chemistry and Physics 75 (2002) 61–66.
[8] C.-W. Nahm, Effect of MnO_2 addition on micro-structure and electrical properties of $ZnO–V_2O_5$-based varistor ceramics, Ceramics International 35 (2009) 541–546.
[9] C.-W. Nahm, Effect of sintering temperature on varistor properties and aging characteristics of $ZnO–V_2O_5–MnO_2$ ceramics, Ceramics International 35 (2009) 2679–2685.
[10] C.-W. Nahm, Preparation and varistor properties of new quaternary Zn–V–Mn–(La,Dy) ceramics, Ceramics International 35 (2009) 3435–3440.
[11] C.-W. Nahm, Influence of Nb addition on micro-structure, electrical, dielectric properties, and aging behavior of MnCoDy modified Zn–V-based varistors, Journal of Materials Science: Materials in Electronics 21 (2010) 540–547.
[12] C.-W. Nahm, Effect of dopant (Al, Nb, Bi, La) on varistor properties of $ZnO–V_2O_5–MnO_2–Co_3O_4–Dy_2O_3$ ceramics, Ceramics International 36 (2010) 1109–1115.
[13] C.-W. Nahm, DC accelerated aging behavior of Co–Dy–Nb doped Zn–V–M-based varistors with sintering process, Journal of Materials Science: Materials in Electronics 22 (2011) 444–451.
[14] C.-W. Nahm, Er_2O_3 doping effect on electrical properties of $ZnO–V_2O_5–MnO_2–Nb_2O_5$ varistor ceramics, Journal of the American Ceramic Society 94 (2011) 3227–3229.
[15] J.C. Wurst, J.A. Nelson, Lineal intercept technique for measuring grain size in two-phase polycrystalline ceramics, Journal of the American Ceramic Society 55 (1972) 109–111.